The Ratio of Toxic-to-Nontoxic miRNAs Predicts Platinum Sensitivity in Ovarian Cancer

Monal Patel[1], Yinu Wang[2], Elizabeth T. Bartom[3,4], Rohin Dhir[5], Kenneth P. Nephew[6], Daniela Matei[2,7], Andrea E. Murmann[1], Ernst Lengyel[5], and Marcus E. Peter[1,3,7]

ABSTRACT

Ovarian cancer remains one of the deadliest gynecologic malignancies affecting women, and development of resistance to platinum remains a major barrier to achieving a cure. Multiple mechanisms have been identified to confer platinum resistance. Numerous miRNAs have been linked to platinum sensitivity and resistance in ovarian cancer. miRNA activity occurs mainly when the guide strand of the miRNA, with its seed sequence at position 2–7/8, is loaded into the RNA-induced silencing complex (RISC) and targets complementary short seed matches in the 3′ untranslated region of mRNAs. Toxic 6mer seeds, which target genes critical for cancer cell survival, have been found in tumor-suppressive miRNAs. Many siRNAs and short hairpin RNAs (shRNA) can also kill cancer cells via toxic seeds, the most toxic of which carry G-rich 6mer seed sequences. We showed here that treatment of ovarian cancer cells with platinum led to increased RISC-bound miRNAs carrying toxic 6mer seeds and decreased miRNAs with nontoxic seeds. Platinum-tolerant cells did not exhibit this toxicity shift but retained sensitivity to cell death mediated by siRNAs carrying toxic 6mer seeds. Analysis of RISC-bound miRNAs in tumors from patients with ovarian cancer revealed that the ratio between miRNAs with toxic versus nontoxic seeds was predictive of treatment outcome. Application of the 6mer seed toxicity concept to cancer relevant miRNAs provides a new framework for understanding and predicting cancer therapy responses.

Significance: These findings demonstrate that the balance of miRNAs that carry toxic and nontoxic 6mer seeds contributes to platinum resistance in ovarian cancer.

Introduction

miRNAs are short 19–22 nucleotide (nt) double-stranded (ds) noncoding RNAs that negatively regulate gene expression. The human genome is estimated to code for approximately 2,300 miRNAs (1). Important regulators of differentiation and development, they are deregulated in virtually all human cancers and can function as tumor suppressors or oncogenes (2–4). miRNA activity involves mainly a very short region of complete complementarity between the "seed" located at positions 2–7/8 of the guide strand (5, 6) and the "seed matches" predominantly located in the 3′ untranslated region (3′ UTR) of targeted mRNAs (7, 8), resulting in gene silencing (9). To function, mature ds miRNA duplexes are loaded onto Argonaute (Ago) proteins forming the RNA-induced silencing complex (RISC; ref. 10). The active miRNA guide strand incorporates into the RISC (10), while the inactive passenger strand is degraded (11).

Epithelial ovarian cancer is one of the deadliest gynecologic malignancies (12). Despite recent improvements in our understanding of ovarian cancer biology (13) and the development of new treatments (14), the vast majority of women with advanced stage ovarian cancer will experience recurrence and succumb to the disease. Most women develop resistance to platinum (Pt) chemotherapy, which is part of the standard first-line treatment for ovarian cancer (15).

Multiple mechanisms have been shown to underlie ovarian cancer treatment resistance (16, 17). A large body of literature supports the role of aberrantly expressed miRNAs in the disease course of ovarian cancer, impacting sensitivity to treatment and long-term treatment outcome. At least 87 miRNAs have been reported to either confer acquired therapy resistance, resensitize ovarian cancer cells to treatment, or to correlate with or predict ovarian cancer treatment outcome (Supplementary Tables S1 and S2). However, there is very little agreement or overlap in those miRNAs identified, raising the question of how this bewildering array of different miRNAs can be linked to therapy resistance in ovarian cancer.

We previously discovered that a large number of siRNAs and short hairpin (sh) RNAs were toxic to all cancer cells independent of their intended target (18). Cells died of simultaneous activation of multiple cell death pathways (18) and could not become resistant to treatment (19). Subsequently, we found that Ago2, a critical component of the RISC, was required for this cell death, and that the toxic si/shRNAs acted like miRNAs by targeting the 3′ UTRs of genes essential for cell survival (20, 21). A 6mer seed present in the guide/antisense strand of the si/shRNA duplex (20) is sufficient for death induced by survival gene elimination (DISE; refs. 20, 22). The DISE concept was recently confirmed for prostate cancer (22).

In an arrayed screen of all possible 4096 6mer seeds in a neutral backbone 19mer siRNA, we determined that the most toxic 6mer seeds were universally high in G nucleotides at the 5′ end of the seed, largely

[1]Department of Medicine/Division Hematology/Oncology, Feinberg School of Medicine, Northwestern University, Chicago, Illinois. [2]Department of Obstetrics and Gynecology, Feinberg School of Medicine, Northwestern University, Chicago, Illinois. [3]Department of Biochemistry and Molecular Genetics, Feinberg School of Medicine, Northwestern University, Chicago, Illinois. [4]Department of Preventive Medicine, Feinberg School of Medicine, Northwestern University, Chicago, Illinois. [5]Department of Obstetrics and Gynecology/Section of Gynecologic Oncology, University of Chicago, Chicago, Illinois. [6]Medical Sciences, Indiana University School of Medicine, Bloomington, Indiana. [7]Robert H. Lurie Comprehensive Cancer Center, Chicago, Illinois.

independent of tissue origin and species (ref. 23 and 6merdb.org). In human cells, we recently identified the seed consensus GGGGGC (targeting the seed match GCCCCC in a miRNA like fashion) as the most toxic seed sequence across three cell lines (21). Toxic 6mer seeds are found in tumor-suppressive miRNAs, including the prototypical tumor suppressive miRNA families, miR-34/449–5p and miR-15/16–5p (23, 24), and we and others have shown that 6mer seed toxicity (6mer seed tox) can be developed for cancer treatment (19, 25). When we treated xenografted ovarian cancer with siRNAs containing toxic seeds, normal tissues were unaffected (19). Various cancer cell lines became more sensitive to 6mer seed tox after EMT was induced or their cancer stemness was increased (26). Both EMT and cancer cell stemness are involved in well-documented mechanisms of chemotherapy resistance (27).

After analyzing miRNAs based on the toxicity of their 6mer seed, we now report that, in cancer cell lines both *in vitro* and *in vivo*, and in tumors from patients with ovarian cancer, the balance of miRNAs containing toxic versus nontoxic seeds strongly associates with the outcome of Pt-based chemotherapy. Analyzing the 6mer seed composition of RISC-bound miRNAs may predict which patients are Pt resistant at the time of initial diagnostic surgery or may acquire Pt resistance.

Materials and Methods

Reagents and antibodies

Carboplatin (#C2538) was purchased from Sigma-Aldrich, cisplatin (#1134357) was from Millipore Sigma, Lipofectamine RNAimax (#13778150) from Thermo Fisher Scientific. Primary antibodies for Western blot analysis: anti-argonaute-2 antibody (#ab32381, RRID: AB_867543) was purchased from Abcam; anti-Dicer (D38E7) antibody (#5362, RRID:AB_10692484) from Cell Signaling Technology; anti-β-actin antibody (#sc-47778, RRID:AB_2714189) was purchased from Santa Cruz Biotechnology. The secondary antibody was a goat anti-rabbit IgG-HRP (#4030–05, RRID:AB_2687483) from Southern Biotech.

Cell lines

Human ovarian cancer cell lines, HeyA8 (received from E. Lengyel, University of Chicago, Chicago, IL; RRID:CVCL_8878), OVCAR5 (obtained from the Developmental Therapeutics Program at the NCI, Rockville, MD; RRID:CVCL_1628), were cultured in RPMI1640 medium (Cell Gro #10–040 CM), supplemented with 10% heat-inactivated FBS (Sigma-Aldrich # 14009C), 1% L-glutamine (Mediatech Inc), and 1% penicillin/streptomycin (Mediatech Inc); PEO1 (RRID:CVCL_2686) and PEO4 (RRID:CVCL_2690) cells both obtained from Sigma-Aldrich were cultured in the above medium and supplemented with 2 mmol/L sodium pyruvate (Mediatech Inc.), 293T WT, 293T Dicer knockout (KO) cells (Clone #2–20; ref. 28), HeLa control (RRID:CVCL_0030) and HeLa Ago2 KO cells were a kind gift from Dr. Sarah Gallois-Montbrun (Univertisy of Paris Descartes, Paris, France; ref. 29), 293T Ago2 KO cells were provided by Dr. Klaas Mulder (Radboud Institute for Molecular Life Sciences, Nijmegen, the Netherlands; ref. 30), and ovarian cancer cell lines A2780 (RRID:CVCL_4862) and A2780R (27) were all grown in DMEM (Gibco #12430054) supplemented with 10% FBS, 1% L-glutamine, and 1% penicillin/streptomycin. All cell lines were authenticated by short tandem repeat profiling at IDEXX BioAnalytics. Cells were used within the first 3–8 passages following thawing, periodically tested for *Mycoplasma* using PlasmoTest (Invitrogen) and were last tested in April 2021.

Assessing cell growth and viability assay

For transfection in 96-well plates to monitor cell growth with IncuCyte Zoom (Essen Bioscience, RRID:SCR_019874), 50 μL Optimem (Thermo Fisher Scientific #331985088) mix containing RNAimax and 10 nmol/L siRNA (siNT1, siGGCAGU or siGGGGGC) was used. RNAimax amounts per 96-well were optimized for each cell line used: A2780 (0.2 μL), PEO1/4 (0.3 μL), HeLa (0.3 μL), 293T (0.1 or 0.2 μL). Seeding densities for reverse transfection with siRNAs or Pt treatment in 96-well plates were also optimized for each cell line used: A2780/A2780R and 293T (1,500 cells), PEO1/PEO4 (5,000 cells), and HeLa (2,000 cells). The following siRNA oligonucleotides were obtained from Integrated DNA Technology and annealed as per the manufacturer's instructions:

siUAGUCG (siNT1) sense: mUmGrGrUrUrUrArCrArUrGrUr CrGrArCrUrArATT
siUAGUCG (siNT1) antisense: rUrUrArGrUrCrGrArCrArUrGr UrArArArCrCrAAA
siGGCAGU (si34a-5p[Seed]) sense: mUmGrGrUrUrUrArCrArUr GrUrArCrUrGrCrCrATT
siGGCAGU (si34a-5p[Seed]) antisense: rUrGrGrCrArGrUrArCrAr UrGrUrArArArCrCrAAA
siGGGGGC sense: mUmGrGrUrUrUrArCrArUrGrUrGrCrCr CrCrCrATT
siGGGGGC antisense: rUrGrGrGrGrGrCrArCrArUrGrUrArAr ArCrCrAAA

For treatment with cisplatin or carboplatin, cells were seeded in triplicates in 96-well plates and treated with the indicated drug concentrations. Cell growth was monitored using IncuCyte Zoom live-cell imaging system (Essen Bioscience) with a 10× objective. The confluency curves were generated using the IncuCyte Zoom software (version 2015A). A viability assay that measures the level of ATP within cells was done in 96-well plates. Briefly, 72 hours posttreatment with drugs or 96 hours post reverse transfection with siRNAs, media in each well was replaced with 70 μL fresh medium and 70 μL of Cell Titer-Glo reagent (Promega #G7570) was added. The plates were covered with aluminum foil and shaken for 5 minutes and then incubated for 10 minutes at room temperature before the luminescence was read on a BioTek Cytation 5. IC_{50} values for cisplatin or carboplatin in a viability assay comparing Pt-sensitive with Pt-tolerant cells were determined using GraphPad Prism 6 software (RRID: SCR_002798) by logarithm normalized sigmoidal dose curve fitting.

Western blot analysis

Cells were lysed using Killer RIPA lysis buffer (150 mmol/L NaCl, 10 mmol/L Tris HCl pH 7.2, 1% SDS, 1% TritonX-100, 1% deoxycholate, 5 mmol/L EDTA) and freshly added phenylmethylsulfonylfluoride (1 mmol/L) and protease inhibitor cocktail (Roche #11836170001). Equal amounts of protein (30 μg) were resolved on a 10% SDS-PAGE gel and Western blot analysis was performed as described previously (20). Visualization of protein bands was performed using the SuperSignal West Dura Extended Duration Substrate (Thermo Fisher Scientific, #34076). Antibodies were diluted in 5% dry milk powder in 0.1% Tween-20/TBS (TBST): anti-argonaute-2 (1:1,000), anti-β-actin (1:5,000), anti-rabbit IgG HRP (1:5,000). Anti-Dicer antibody was diluted (1:1,000) in 5% BSA in TBST.

miR-21-5p inhibition and real-time PCR

Real-time PCR was performed for miR-21-5p in A2780R cells infected with lentivirus Zip control (pLenti-III-miR-GFP control vector from Applied Biological Materials #m001) or Zip-21

(LentimiRa-GFP-hsa-miR-21–5p vector, Applied Biological Materials #mh10276). Briefly, 25 ng total RNA was used to make cDNA using the High-Capacity cDNA Reverse Transcription Kit (Applied Biosystems #4368814). The qPCR was then done using the Taqman Gene Expression Master Mix (Thermo Fisher Scientific #4369016) as described previously (31) using the following primers: hsa-miR-21 (Thermo Fisher Scientific, #0003970) and Z30 (Thermo Fisher Scientific, #001092). The relative expression of miR-21-5p was normalized to the level of Z30. Statistical analysis was performed using Student t test.

Small total RNA sequencing

For small (sm)RNA-sequencing (RNA-seq) experiments, cells were lysed using QIAzol. For all RNA-seq samples, a DNAse digestion step was included using the RNAse-free DNAse set (Qiagen #79254). Total RNA was isolated using the miRNeasy Mini Kit (Qiagen # 74004). The quality of RNA was determined using an Agilent Bioanalyzer. The RNA library preparation and subsequent sequencing on Illumina HiSEQ4000 was then done by the NU-Seq Core at Northwestern University (Chicago, IL).

Raw read sequences were trimmed with trim_galore to remove all standard Illumina adapters, leaving reads at least 6 bp in length. In addition, any reads containing the substring GTCCGACGATC followed by 3 to 5 nucleotides were discarded. This removed any remaining 5′ adapter sequences and ensured that only RISC-bound sRNAs were analyzed, which was crucial for determining position 2–7 of each read. Trimmed reads were then sorted, uniq'd, counted. A six-nucleotide Unique Molecular Identifier (UMI) was removed from each read, and the numbers of reads associated with the same core read sequence and any UMI were summed to generate the raw read count for a particular sample. Counts were tabulated for each read and sample and normalized per million reads in the column (sample) sum. Reads were blasted (blastn-short) against custom blast databases created from all processed human miRNAs (miRbase 22.1, RRID: SCR_017497) and from the most recent RNA world database (human_and_virus_vbrc_all_cali_annoDB_sep2015) obtained from the Tuschl lab at Rockefeller University (New York, NY). Processed miRNA hits were filtered for 100% identity, and a match length of at least 18 bases. RNAworld hits were filtered for at least 95% identity, with the match starting within the first 9 bp of the sequencing reads. These filtered blast results were used to annotate reads with their likely source, and when no blast hit passed these filters, the read was annotated "noMatch." Reads were also associated with their 6mer seed (positions 2–7) and with the previously identified seed toxicity determined in human ovarian cancer cells HeyA8 (6merdb.org; ref. 23). For tractability, only reads with a total count of at least 6 CPM summed across all samples were retained for further analyses. To identify reads enriched in a particular group of samples, we used the R package EdgeR (RRID:SCR_012802) with the un-normalized read counts, annotating the resulting reads with seed toxicity and blast-based annotation as described above.

Ago pull-down and subsequent small RNA-seq

For Ago pull-down experiments, transfections or treatments described above for 96-well plates were scaled up for 150 mm dishes. At the required time point for pull-down, cells were washed with PBS and 10 million cell pellets were frozen at -80 °C until ready to be lysed using 1 ml NP40 lysis buffer [50 mmol/L Tris pH 7.5, 150 mmol/L NaCl, 5 mmol/L EDTA, 0.5% NP-40, 10% (v/v) glycerol, 1 mmol/L NaF; supplemented with 1:200 EDTA-free protease inhibitors (Millipore #539134) and 1:1000 RNaisin Plus (Promega #N2615) before use]. Mouse or patient tumor lysates were prepared by first chopping 250 mg tissue with a clean razor blade and then using a Dounce homogenizer containing 1 ml NP40 lysis buffer. In a few patient tumors for which 250 mg tissue was not available, at least 100 mg tissue was used for pull down. The tissue was homogenized by passing the pestle up and down the cylinder several times while keeping the homogenizer cool on ice. Cell or tissue lysates were then incubated on ice for 15 minutes, vortexed, and then centrifuged at $20,000 \times g$ for 20 minutes. The lysates were then transferred to siliconized micro-centrifuge tubes (low-binding, Eppendorf #022431021), and Ago1–4 were pulled down using 500 μg of Flag-GST-T6B peptide (32) and with 80 μL anti-Flag M2 Magnetic beads (Sigma #M8823) for 3 hours on a rotor at 4°C. The precipitate was washed three times in NP40 lysis buffer and during the last wash, 10% of the beads were removed and incubated at 95°C for 5 minutes in 2× SDS-PAGE sample buffer. The efficiency of the pull down was determined by running these samples on a 10% SDS-PAGE gel, transferring them to nitrocellulose membrane and immunoblotting against Ago2 (Abcam #32381). Five-hundred microliters of TRIzol reagent was added to the remaining beads and RNA was extracted using the manufacturer's instructions. The RNA pellet was dissolved in 20 μL water. Half of the RNA sample was dephosphorylated with 0.5 U/μL of CIP alkaline phosphatase at 37°C for 15 minutes and then radiolabeled with 0.5 μCi γ-^{32}P-ATP and 1 U/μL T4 PNK kinase for 20 minutes at 37°C. The RNAs interacting with Ago1–4 were visualized on a 15% Urea-PAGE. The other half of the RNA sample was used for a small RNA library preparation, using Illumina primers (RRID:SCR_010233) as described previously (33). Concisely, RNA was ligated with 3′-adenylated adapters and separated on a 15% denaturing Urea-PAGE. The RNA corresponding to insert size of 19–35 nt was eluted from the gel using radiolabeled size markers, ethanol precipitated and then ligated with the 5′ adapter. The RNA samples were then separated on a 12% Urea-PAGE, extracted from the gel and reverse transcribed using Superscript III reverse transcriptase (Invitrogen #18080–044) and the cDNA was amplified by PCR. The cDNA was sequenced on Illumina Hi-Seq 4000.

RNA size marker sequences used for smRNA library preparation

19nt RNA size marker: rCrGrUrArCrGrCrGrGrGrUrUrUrArArArCrGrA.

35nt RNA size marker: rCrUrCrArUrCrUrUrGrGrUrCrGrUrArCrGrCrGrGrArArUrArGrUrUrUrArArArCrUrGrU

The following set of eight 3′ adenylated adapters was used, each containing a unique 6mer barcode sequence at the 5′ end (underlined). These barcodes were used to separate the reads into individual pull-down samples before proceeding with the small RNA pipeline as described above. For ease of use, the sequence files uploaded to GEO have already been split into reads from individual experiments:

Adapter GG-L	1-rAppNN<u>CTGACA</u>TGGAATTCTCGGGTGCCAA
Adapter GG-L	2-rAppNN<u>ACTAGC</u>TGGAATTCTCGGGTGCCAA
Adapter GG-L	3-rAppNN<u>GTACGT</u>TGGAATTCTCGGGTGCCAA
Adapter GG-L	4-rAppNN<u>TGTACG</u>TGGAATTCTCGGGTGCCAA
Adapter GG-L	5-rAppNN<u>CAGCAT</u>TGGAATTCTCGGGTGCCAA
Adapter GG-L	6-rAppNN<u>TCATAG</u>TGGAATTCTCGGGTGCCAA

Adapter 7-rAppNNATAGTATGGAATTCTCGGGTGCCAA
GG-L
Adapter 8-rAppNNGATGCTTGGAATTCTCGGGTGCCAA
GG-L
5′ adapter with unique molecular identifiers (UMI): GTTCA
GAGTTCTACAGTCCGrAr CrGrArUrCrNrNrNrN
5′ adapter without UMI: rGrUrUrCrArGrArGrUrUrCrUrArCrAr
GrUrCrCrGrArCrGrArUrC (used only in the experiment shown
in **Fig. 3**).

RT primer sequence: GCCTTGGCACCCGAGAATTCCA
Four 3′ PCR primers were used each containing a unique index
(underlined) recognized by Illumina:

Primer1:CAAGCAGAAGACGGCATACGAGATCGTGATGT
GACTGGAGTTCCTTGGCACCCGAGAATTCCA
Primer2:CAAGCAGAAGACGGCATACGAGATACATCGGT
GACTGGAGTTCCTTGGCACCCGAGAATTCCA
Primer3:CAAGCAGAAGACGGCATACGAGATGCCTAAGT
GACTGGAGTTCCTTGGCACCCGAGAATTCCA
Primer4:CAAGCAGAAGACGGCATACGAGATTGGTCAGT
GACTGGAGTTCCTTGGCACCCGAGAATTCCA
5′PCR primer:
AATGATACGGCGACCACCGAGATCTACACGTTCAGAG
TTCTACAGTCCGA

The seed tox graph

Reads were aggregated (read numbers collapsed) first by the seed
sequence (position 2–7 of each read) and then by the miRNA and RNA
World RNA that the read aligned to (Blast search see above). Each seed
sequence had an assigned percent cell viability from the 4096 siRNA
screen in the ovarian cancer cell line HeyA8 (ref. 23 and 6merdb.org),
the aggregated read numbers were further binned in RStudio based on
the HeyA8 cell viability in 1% increments/bins. Seed tox graphs
(number of reads on y-axis and 6mer seed viability on x-axis) were
then generated using Excel with smoothing enabled. The file with the
collapsed data was used to identify the most abundant miRNAs that
make up each peak in the 6mer seed tox graph. When a peak consisted
of more than one abundant miRNA (>5,000 or >1,000 reads) miRNAs
were listed in the order of abundance.

Analysis of smRNAs in normal tissues

Data of total smRNA were retrieved (accession #GSE11879) and
analyzed from 9 human tissues. To compare different tissues and
consistently identify and label the most abundant miRNAs, all 9 data
sets were normalized to 1,000,000 reads. For each tissue, miRNAs were
labeled in seed tox graphs with >5,000 norm average reads. When a
peak contained more than one miRNA they are shown in the order
from highest to lowest abundance.

Seed and tox analysis

To determine the average seed tox of all reads in a data set or to
determine the average 6mer seed composition of reads in a dataset,
numbers for all individual reads were divided by a factor that reduced
the number of the most abundant read to less than 1,000. In a
comparison analysis, significantly up- or downregulated reads were
processed separately. Associated toxicity and 6mer seed sequences for
each read were then multiplied by this factor using a Perl script. The
resulting read numbers were plotted as a box and whisker plot using
the chart function of StatPlus:Mmac Pro v.7.3.3. with default settings:
the mean is shown in red, the median in blue. The upper and lower

limits of the box indicate the upper and lower quartile, respectively.
The ends of the whiskers indicate the minimum and maximum,
respectively and green dots show outliers. P values of deregulated
seed toxicities were determined using a Kruskal–Wallis median rank
test. Expanded seed sequences were plotted using Weblogo (http://
weblogo.berkeley.edu, RRID:SCR_010236) as a custom frequency
plot.

Comparison of total and RISC-bound short RNAs

RNA-seq datasets were used for either total smRNA (GSE165148
for A2780 and GSM3029765/GSM3029766 for HeyA8) or Ago-bound
smRNAs (GSE165148 for A2780 and GSM3029217/GSM3029218 for
HeyA8). To compare the amount of total versus RISC-bound miRNAs
all four datasets (with two duplicates each) were combined into one file
using R. Each read column was renormalized to 1,000,000 reads. All
reads were isolated with a length of 19–25 nt before generating Seed
Tox graphs. For statistical analysis in **Fig. 2A** and **B**, cumulative
distribution functions of viabilities across all reads were compared
using the Kolmogorov–Smirnov test.

In vivo treatment of OVCAR5 cells with carboplatin

Note: while OVCAR5 cells were recently suggested to be of upper
gastrointestinal origin (34), these cells were originally isolated from
ascites of a patient with metastatic ovarian cancer (35) and when
grown intraperitoneally *in vivo* show the histology of high-grade
ovarian cancer (36, 37). Xenografting them intraperitoneally and
treating them with carboplatin is therefore relevant to the treatment
of ovarian cancer. In addition, while studied here in the context of
ovarian cancer, the 6mer seed tox concept is applicable to all cancer
types. Animal studies were conducted according to a protocol
(#IS00003060) approved by the Institutional Animal Care and Use
Committee of Northwestern University. Female (6–8 weeks old)
athymic nude mice ($Foxn1^{nu}$, Envigo) were injected intraperitoneally
with 2 million OVCAR5 ovarian cancer cells to induce tumors. After
2 weeks inoculation (38), mice were treated intraperitoneally with PBS
(control, mice ID: 791, 792, 793, 794, $n = 4$), or 25 mg/kg carboplatin
($n = 5$) in the following treatment regimens: once-a-week for 3 weeks
(stage 1, $n = 2$, mice ID: 795, 797); 3-week carboplatin followed by two-
week no drug recovery (stage 2, $n = 1$, mice ID: 796); additional two
weeks (5 weeks carboplatin in total) carboplatin after recovery (stage 3,
$n = 2$, mice ID: = 798, 800). Xenograft tumors were collected 1 week
after carboplatin treatment and processed for cancer cell isolation and
RNA extraction. Tumors were mechanically and enzymatically dis-
sociated in DMEM/F12 (Thermo Fisher Scientific, Ref# 11320) con-
taining collagenase (300 IU/mL, Sigma-Aldrich, catalog no. C7657)
and hyaluronidase (300 IU/mL, Sigma-Aldrich, catalog no. H3506) for
2 hours at 37°C. Red blood cell lysis used RBC lysis buffer (BioLegend,
catalog no. 420301), followed by DNase (1 mg/mL, Sigma Aldrich,
catalog no. DN25) treatment and filtering through a 40-μm cell
strainer (Thermo Fisher Scientific, catalog no. NC0147038) to produce
single-cell suspension. EasySep Human Epcam Positive Selection Kit
(StemCell Technologies, catalog no. 17846) was used on the single-cell
suspension for Epcam-positive ovarian cancer epithelial cell selection
following manufacturer's instructions.

Patient samples and analysis

All patient samples (described in Supplementary Table S3) were
collected at the University of Chicago Medical Center following
approval from the Institutional Review Board, and after obtaining
written informed consent from the patients. The studies were con-
ducted in accordance with recognized ethical guidelines. All patients
included in the study underwent primary debulking surgery for

advanced stage metastatic high-grade serous ovarian cancer by a gynecologic oncologist. All patients received multiple cycles of a combination of taxane and Pt. None of the patients had received a PARP inhibitor. The tissue was snap frozen at the time of surgery and stored at -80°C until further use. Clinicopathologic data was collected prospectively and updated every three months based on clinical exam, CA-125, or imaging.

Analysis of correlation between patient groups and seed tox

Two cohorts of patients were compared: Group I: 9 patients were Pt refractory or resistant (recurrence <180 days after the end of chemo = Pt-R patients), Group II was platinum sensitive, experiencing a late recurrence (>180 days) or no recurrence [= Pt-sensitive (Pt-S) patients]. Total norm count data were used. Reads were aggregated according to 6mer seed and blasted miRNAs. Patients were either separated into the two groups (Pt-R and Pt-S) compared or read associated toxicity was correlated using Pearson correlation (including P values) with Pt-S days as given in Supplementary Table S3.

Identification of the most abundant miRNAs enriched in Pt-R patients

Total norm count data after adapter removal were used. Reads were aggregated (multiple rows were collapsed into one) according to 6mer seed and blasted miRNAs. Student t test ($P < 0.05$) was used to identify all miRNAs that were enriched in the Pt-R patients (>1.5×). To focus on only highly expressed reads, reads with an average read number of 1,000 or more across all samples were used for this analysis. The highest number of reads across all samples was 13,681 for miR-125b with the seed CCCUGA.

Unsupervised hierarchical cluster analysis and heatmaps

The most abundant miRNAs (>10,000 Ave reads across all samples; Supplementary Fig. S9F) were hierarchically clustered and plotted in R according to pairwise Pearson correlation.

Kaplan–Meier analysis

Samples were divided into two groups according to expression of particular seeds/miRNAs, and survfit/ggsurvplot was used in R to create Kaplan–Meier curves contrasting the time to recurrence between the two groups.

Statistical analyses

IncuCyte experiments were performed in triplicate, and the data expressed as mean ± SE. Continuous data were compared using t tests for two independent groups. For evaluating continuous outcomes over time, two-way ANOVA was performed using the Stata1C software. Treatment condition was used as a component of primary interest and time as a categorical variable. When controls were very different between different treated cells, a binomial test was used for comparisons of single proportions to hypothesized null values (23).

Data availability

smRNA-seq data were deposited at GEO under the GSE series GSE165148.

Results

Both toxic siRNAs and carboplatin exert toxicity through RNAi

We decided to use the two highly toxic seeds, GGCAGU (found in miR-34a-5p) and GGGGGC (found in miR-1237–5p), embedded in an siRNA to probe cells. Both siGGCAGU and siGGGGGC were more

toxic to Dicer-deficient 293T than wt cells (Supplementary Fig. S1A–S1C). We concluded that both siRNAs killed cells through RNAi, because both showed severely reduced toxicity to Ago2 KO HeLa cells, yet were highly toxic to wt HeLa cells (Supplementary Fig. S1D). Similarly, these two siRNAs were also more toxic to wt than to Ago2 KO 293T cells (Supplementary Fig. S1E). We previously reported that HCT116 cells deficient for either Drosha or Dicer, which are devoid of most canonical miRNAs, were hypersensitive to 6mer seed tox and carboplatin (20, 23). We now show that Dicer KO 293T cells are also much more sensitive to the toxic effects of clinically used carboplatin (Supplementary Fig. S1F) while isogenic Ago2 KO 293T cells showed a reduced susceptibility to the toxicity of carboplatin (Supplementary Fig. S1G). These data suggest that the composition of RISC-bound miRNAs and RNAi not only determines the activity of toxic siRNAs but, at least in part, the sensitivity of cells to Pt.

Platinum-tolerant ovarian cancer cells are sensitive to 6mer seed tox

To determine whether 6mer seed tox contributes to the response of OC cells to Pt, we first tested two cell line pairs representing a Pt-S and Pt-R phenotype, respectively. A2780R cells were made resistant by culturing A2780 cells for 5 cycles with increasing concentrations of cisplatin (39). PEO1 and PEO4 cells were derived from the same patient at different times after combination chemotherapy with cisplatin, chlorambucil, and 5-fluorouracil (40). PEO1 were reported to have a hemizygous BRCA2 mutation (41) and PEO4 (BRCA2 wildtype reversion mutation) was a later isolate, taken from the patient after her second relapse and hence more resistant to Pt drugs. Treatment of the A2780 cell pair with cisplatin confirmed that the A2780R cells were more resistant to cisplatin than the parental cells (**Fig. 1A** and **B**). Interestingly, A2780R cells were at least as sensitive to both siGGCAGU and siGGGGGC as the parental cells (**Fig. 1C** and **D**). A similar phenomenon was observed when the PEO1/4 cell pair was treated with carboplatin or toxic siRNAs (**Fig. 1E–H**). These data suggest that 6mer seed tox can kill platinum-resistant ovarian cancer cells.

Presenting the miRNA space as a function of seed toxicity—the seed tox graph

Interestingly, many seemingly unrelated miRNAs share seeds of similar toxicity. Therefore, we developed a graphical representation of all miRNAs in cells or tissues at their actual expression levels, plotting the miRNAs according to their seed toxicities (the seed tox graph). When comparing miRNA expression in different human tissues, we found that most tissues express predominantly nontoxic seedcontaining miRNAs (Supplementary Fig. S2), and only a small fraction of miRNAs had a predicted seed with high toxicity. A few abundant miRNAs are expressed across all tissues (Supplementary Fig. S2). These include the highly toxic miRNAs 22–3p and 24–3p (red), the intermediately toxic miRNAs miR-126–3p, miR-23b-3p, miR-29a-3p (blue), and the nontoxic miRNA members of the let-7 family, miR-125b-5p, and miR-21–5p (green).

Enrichment of miRNAs in the RISC in ovarian cancer cells

miRNAs in cancer are almost always studied by quantifying them in the total RNA fraction. However, previous reports demonstrated that most mature miRNAs are not Ago associated (42) and that endogenous miRNAs vary widely in their level of RISC association (43, 44). To assess the 6mer seed tox of biologically relevant miRNAs, we pulled down all Ago proteins and their associated miRNAs (20) from two ovarian cancer cell lines, allowing us to
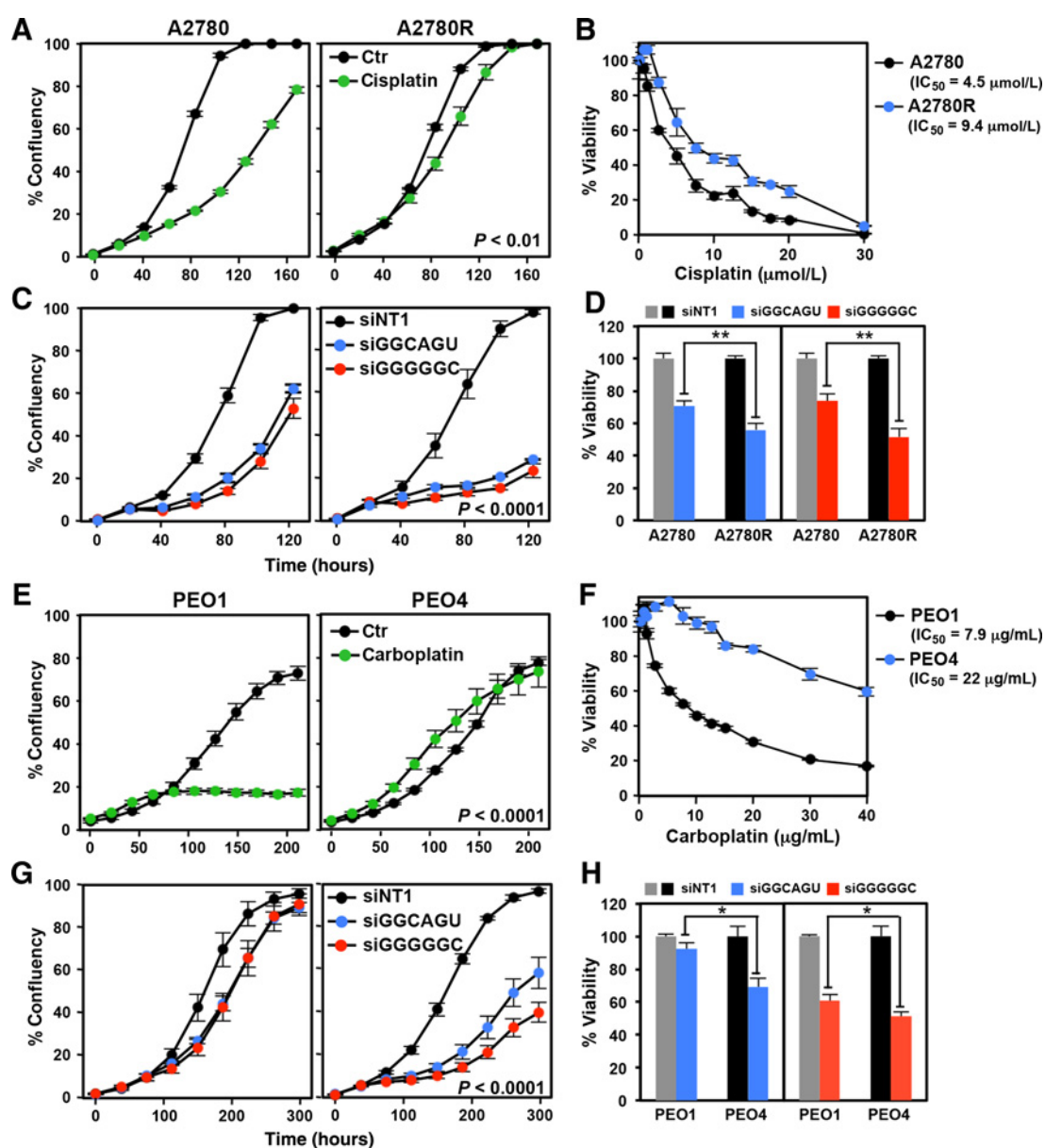
Figure 1.
Platinum-tolerant Pt-R ovarian cancer cells are at least as sensitive to toxic 6mer seeds as Pt-S cells. **A,** Change of confluency of A2780 and A2780R cells over time treated with PBS or 5 μmol/L cisplatin. **B,** Dose–response curves (72-hour ATP viability assay) of cells in **A**. **C,** Change of confluency of A2780 and A2780R cells over time treated with either 10 nmol/L siNT1, siGGCAGU, or siGGGGGC. **D,** Viability of the cells in **C** 96 hours after transfection with 10 nmol/L of the siRNAs. **E,** Change of confluency of PEO1 and PEO4 cells over time treated with water or 1 μg/mL carboplatin. **F,** Dose–response curves (72-hour ATP viability assay) of cells in **E**. **G,** Change of confluency of PEO1 and PEO4 cells over time treated with either 10 nmol/L siGGCAGU or siGGGGGC. **H,** Viability of the cells in **G** 96 hours after transfection with 10 nmol/L of the siRNAs. Each data point (**A**, **B**, **C**, **E**, **F**, and **G**) represents mean ± SE of three replicates. Each bar (**D** and **H**) represents ± SD of three replicates. *P* values were calculated using ANOVA (**A**, **C**, **E**, and **G**), or Student *t* test (**D** and **H**). *, $P < 0.05$; **, $P < 0.001$.

determine the exact positions 2–7 of RISC-bound guide strands. The results were compared with the analysis of total small RNAs in a seed tox graph with the x-axis showing the seed toxicity (**Fig. 2A** and **B**). The two pairs of graphs were significantly different. A number of miRNAs were highly enriched in the RISC-bound fraction of both cell lines. These included the toxic miRNAs 22–3p and 24–3p and the nontoxic miRNA miR-125b-5p (**Fig. 2**). In addition, members of the toxic miRNA family miR-15/16, miR-15a/b-5p and miR-424–5p were also highly enriched (**Fig. 2C**).

Other miRNAs, most notably the highly abundant members of the let-7–5p family, were reduced in the RISC (**Fig. 2C**). It was also recently reported that many of these miRNAs had a different presence in the RISC than in the total RNA fraction of 293T and A549 cells (asterisks in **Fig. 2C**; ref. 43). This analysis demonstrates that analyzing RISC-bound miRNAs, rather than quantifying total miRNA levels, will more accurately assess functionally relevant miRNAs, which is critical for the analysis of 6mer seed tox. We, therefore, used these techniques in the subsequent experiments.
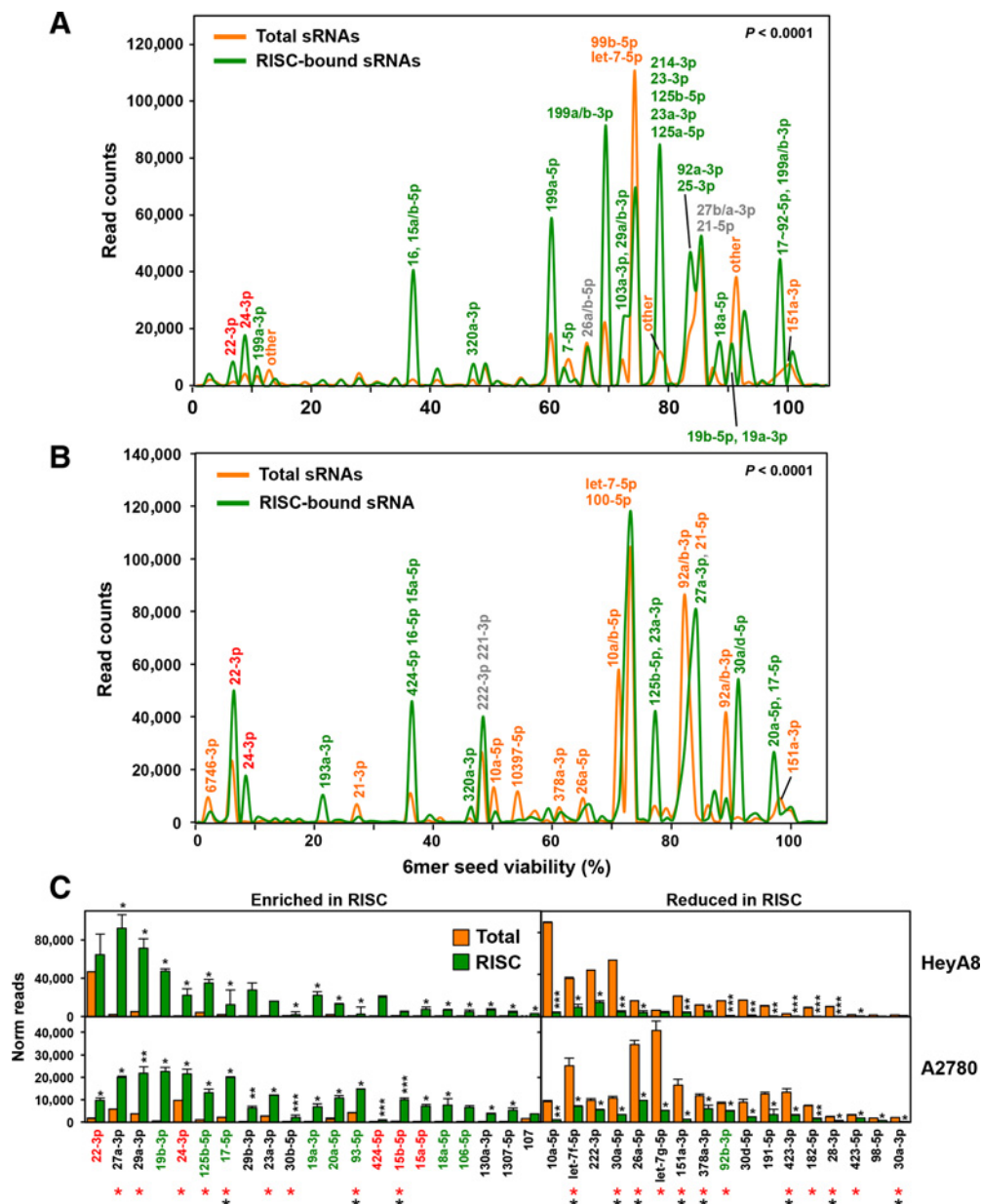
Figure 2.
Selective uptake of miRNAs into the RISC of ovarian cancer cells. **A** and **B,** miRNA seed tox plots of either RISC-bound or total miRNAs in A2780 (**A**) and HeyA8 (**B**) cells. miRNAs that contribute to peaks with >5,000 reads are labeled. For each labeled peak, miRNAs are listed in the order of abundance. The percentage of miRNAs bound to the RISC was higher than the percentage of miRNAs in the total short (s)RNA populaton (79%/88.2% total and 97.6%/96.3% RISC bound in A2780 and HeyA8 cells, respectively). The seed viability (*x*-axis) for HeyA8 cells was used (6merdb.org). The significance of the difference between total and RISC-bound small RNAs was established by performing a Kolmogorov–Smirnov test. Actual *P* values were: A: D = 0.13 (*P* ≪1 × 10^{-15}) B: D = 0.11 (*P* ≪1 × 10^{-15}). **C,** All miRNAs with an average read number of >1,000 in either cell line and >1.5 fold enriched (left) or reduced (right) in the RISC ranked according to the combined read numbers (total and RISC). Student *t* test *P* values are shown; *, *P* < 0.05; **, *P* < 0.001; ***, *P* < 0.0001. miRNAs with toxic seeds are shown in red and putative protective miRNAs with nontoxic seeds are shown in green. miRNAs that have been reported before to be enriched or depleted in the RISC in the same way in either 293T (red asterisks) or A549 (black asterisks; ref. 43) are labeled.

Changes in RISC composition related to short- and long-term treatment with platinum

Next, we determined the toxicity of RISC-bound miRNAs in Pt-S ovarian cancer cells short-term treated with Pt-based chemotherapy or in Pt-R (long-term treated) cells (**Fig. 3**). The RISC of A2780 (Pt-S) and A2780R (Pt-R) cells untreated or treated with cisplatin for 72 hours (a

time point before the onset of cell death) was pulled down and the toxicity of all detected miRNAs plotted (**Fig. 3A**). In short-term cisplatin-treated A2780 cells, highly toxic RISC-bound miRNAs (viability <20%), including miR-22/24–3p, were significantly upregulated, while miRNAs with nontoxic seeds (viability >80%) were downregulated (**Fig. 3D**). The cisplatin-induced increase in toxic miRNAs was
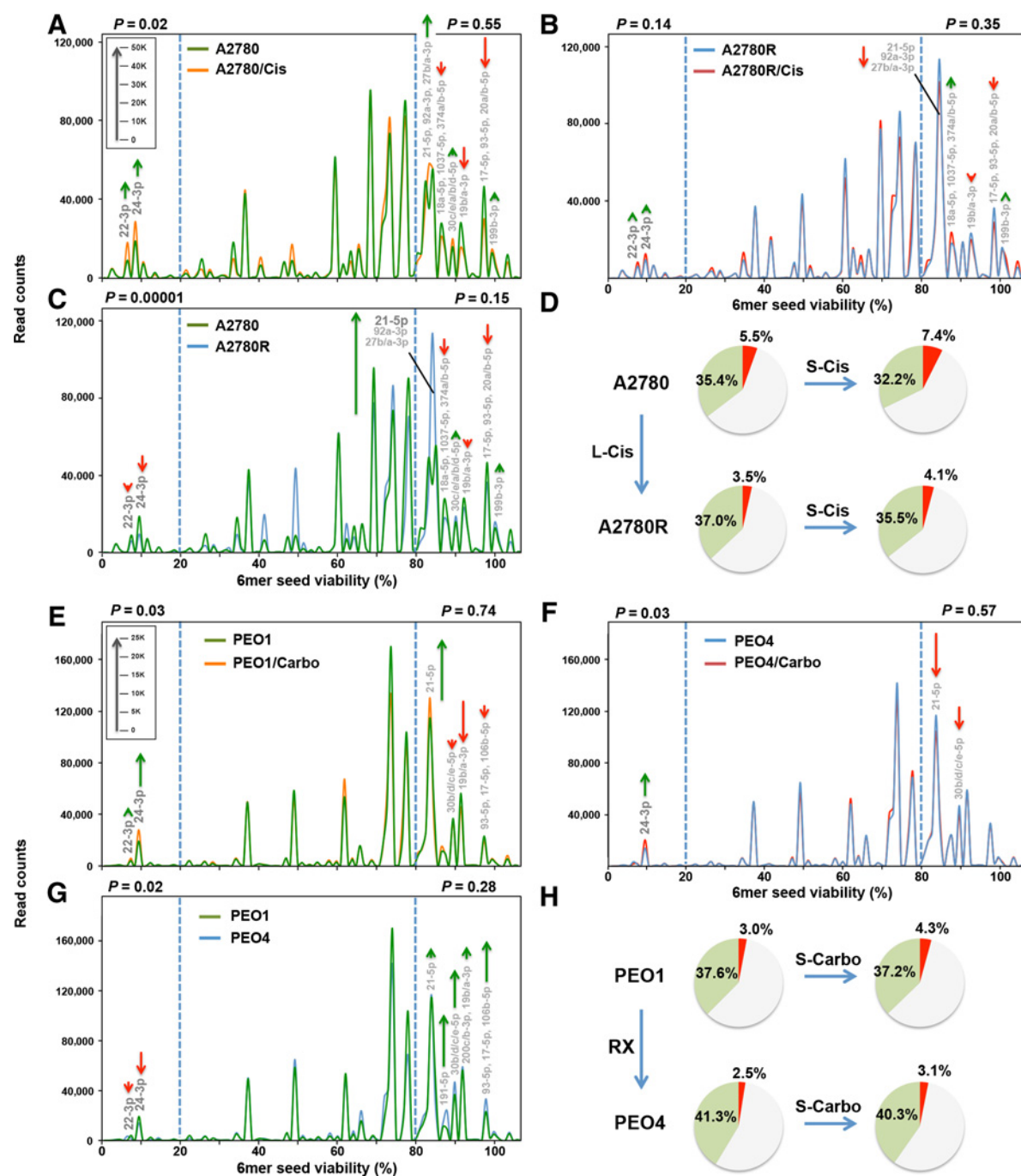
Figure 3.
Change in seed toxicity of RISC bound miRNAs in ovarian cancer cells exposed to platinum. **A** and **B,** RISC-bound sRNA seed tox graphs of A2780 (**A**) or A2780R (**B**) cells treated with 5 μmol/L cisplatin or PBS for 72 hours. Green arrows, net increase, and red arrows, net decrease of >1,000 reads in peak in cisplatin (Cis)-treated cells, respectively. **C,** RISC-bound sRNA seed tox graphs of PBS-treated A2780 and A2780R cells. Green arrows, net increase, and red arrows, decrease of >1,000 reads in peak in A2780R cells, respectively. **D,** RISC composition of A2780 cells or cells made resistant with long-term treatment with cisplatin (A2780R). Shown are pie charts of short-term (S-Cis)– or long-term (L-Cis)–treated cells. Reads with a predicted 6mer seed viability of <20% are shown in red, >80% in green, and in between in gray. **E,** RISC-bound sRNA seed tox graphs of PEO1 cells treated with 1 μg/mL carboplatin (Carbo) or water for 72 hours. Green arrows, net increase, and red arrows, net decrease of >1,000 reads in peak in carboplatin-treated cells, respectively. **F,** RISC-bound sRNA seed tox graphs of PEO4 cells treated with 1 μg/mL carboplatin or water for 72 hours. **G,** RISC-bound sRNA seed tox graphs of water-treated PEO1 and PEO4 cells. Green arrows, net increase, and red arrows, decrease of >1,000 reads in peak in PEO4 cells, respectively. **H,** RISC composition of PEO1 or PEO4 cells. Shown are pie charts of short-term (S-Carbo)– or long-term (RX)–treated cells isolated from patients. Reads with a predicted 6mer seed viability of <20% are shown in red, >80% in green, and in between in gray. *P* values were calculated using pairwise comparisons of all reads in the two different treatments in two groups: reads with predicted viability >80% and <20% (blue stippled lines). In these areas, the most significantly changed miRNAs are labeled. The average miRNA content of RISC-bound sRNAs across all A2780/PEO samples was 97.6%/97.8%, respectively. Length of green and red arrows corresponds to number of reads (insets in **A** and **E**).

no longer significant in the Pt-R A2780R cells (**Fig. 3B**). We then compared the RISC content between Pt-S and Pt-R cells (**Fig. 3C**). The A2780R cells contained fewer toxic miRNAs and more nontoxic miRNAs in the RISC compared with the Pt-S cells (**Fig. 3D**). A striking difference between the Pt-S and Pt-R cells was the increase in miR-21–5p in the Pt-R cells (**Fig. 3C**; Supplementary Fig. S3A). Inhibiting miR-21-5p (Supplementary Fig. S3B) rendered Pt-R cells more sensitive to cisplatin (Supplementary Fig. S3C). Most of these specific changes were not seen when the toxicity of total miRNAs was analyzed (Supplementary Fig. S4A and S4B) validating this approach of analyzing RISC-bound miRNAs. Pt treatment of PEO1 cells, as with treatment of A2780 cells, resulted in a significant increase of RISC-bound toxic miRNAs, including 22/24–3p (**Fig. 3E**). This increase was not found in the Pt-R PEO4 cells (**Fig. 3F**). Again, the toxic miRNAs were significantly underrepresented in the RISC of the Pt-R PEO4 cells when compared with PEO1 cells (**Fig. 3G**). Similar changes in the balance between toxic and nontoxic RISC-bound miRNAs were therefore found in both ovarian cancer cell line pairs (**Fig. 3D** and **H**). However, nontoxic miRNAs, other than miR-21–5p, were upregulated in the resistant PEO4 cells (green arrows in **Fig. 3G**). The data suggest that the ratio between miRNAs with toxic versus nontoxic 6mer seeds determines sensitivity to Pt in the ovarian cancer cell lines.

To determine whether the changes detected in cell lines treated *in vitro* can also be found in the RISC of tumors grown in mice and treated with Pt, we injected OVCAR5 cancer cells orthotopically into nude mice and treated them repeatedly with either PBS or carboplatin (Supplementary Fig. S5A). OVCAR5 tumors treated with carboplatin were in general smaller compared with those of PBS injected control animals (insert a in Supplementary Fig. S5B). Consistent with the cell line models of acquired Pt resistance, *in vivo* Pt-treated Pt-sensitive OVCAR5 tumors showed a reduction of toxic RISC-bound miRNAs with an increase in nontoxic miRNAs (Supplementary Fig. S5C). The most apparent increase of a nontoxic miRNA was in miR-194-5p (Supplementary Fig. S5B and S5C). This increase correlated with the degree of Pt resistance of the tumors isolated from the carboplatin-treated mice (insert b in Supplementary Fig. S5B) and supports our hypothesis that cancer cells have different ways to acquire therapy resistance through upregulation of various miRNAs with nontoxic 6mer seeds.

Uptake of toxic siRNAs into the RISC of Pt-tolerant cells

To determine why the Pt resistant cells were more sensitive to toxic 6mer seed containing siRNAs, we transfected the A2780/A2780R cell pair with a low amount (1 nmol/L) of the nontoxic siUAGUCG (siNT1) or either of the toxic siGGCAGU or siGGGGGC siRNAs. At this concentration, the latter two siRNAs were not toxic to the parental cells but significantly reduced cell growth of the Pt-R cells (Supplementary Fig. S6A). All transfected cells had large numbers of RISC-bound and total reads derived from the guide strand of the transfected siRNAs (Supplementary Fig. S6B). There were few reads derived from the blocked passenger strand (Supplementary Fig. S6C). We noticed an equal uptake of the nontoxic siRNA into Pt-S and Pt-R cells and their RISC with a higher uptake of the two toxic siRNAs into the RISC of A2780R cells compared with A2780 cells (**Fig. 4A–D**) but only a slightly higher increase of the two toxic siRNAs in the total smRNA of the Pt-R cells (Supplementary Fig. S6D–S6G).

On the basis of these results, we were able to assess the ratio of toxic siRNA to RISC-bound miRNA required to reduce cell growth. Because Ago2 KO cells are resistant to the effects of toxic siRNAs, we know that

the toxicity is dependent on the presence of Ago2 in the RISC. The nontoxic siUAGUCG replaced about the same amount of miRNAs from the RISC in Pt-S and Pt-R cells, while the two toxic siRNAs were less efficient in replacing miRNAs in the Pt-S cells (**Fig. 4D**). The overall seed toxicity of all RISC-bound reads in cells transfected with the two toxic siRNAs significantly dropped in A2780R cells, resulting in a relatively small change in overall 6mer seed composition of RISC-bound short (s)RNAs between the A2780 and A2780R cells (**Fig. 4E**). These data suggest that a moderate shift of seed toxicity of about 10% or less is sufficient to reduce cell growth and/or cause cell death in response to Pt.

Changes in tumors of patients with ovarian cancer caused by Pt-based therapy

To determine whether changes in toxic and nontoxic 6mer seed containing miRNAs are associated with differences between patients with Pt-sensitive and Pt-resistant ovarian cancer, we studied a well characterized group of Pt-sensitive and Pt-resistant patients with FIGO stage III/IV high-grade serous ovarian cancer who underwent primary debulking surgery followed by adjuvant chemotherapy with carboplatin and paclitaxel (Supplementary Table S3). Fresh frozen primary ovarian cancer tissue specimens were subjected to an Ago pull-down/smRNA-seq analysis. Two cohorts of patients were compared: Group I: Pt resistant; Group II: Pt sensitive (**Fig. 5A**). Because the RISC composition could be affected by the age of the patients, both groups were age matched (**Fig. 5B**). miRNA enrichment in the pulled down RISC was highly efficient. Across all 21 samples, between 97.4% and 98.1% of all Ago-bound reads were miRNAs. When ranking all highly abundant reads derived from miRNAs (sum >10,000 across all samples) according to the fold change in the Pt-S patients, we found that tumors in Pt-S patients had an enrichment of miRNAs with more toxic seeds while Pt-R tumors were enriched in miRNAs with nontoxic seeds (**Fig. 5C**). This correlation was also apparent when all ∼38,000 reads were ranked according to the predicted 6mer seed tox of each read (**Fig. 5D**). A shorter time to relapse correlated with higher amounts of nontoxic RISC-bound miRNAs.

Comparing the significant differences in RISC-bound miRNAs between the two groups in a seed tox graph identified miR-449a and miR-150-5p as depleted and several miRNAs as enriched (e.g., miR-125a/b) in Pt-R tumors (**Fig. 5E**). That RISC-bound miRNAs enriched in the Pt-R tumors had a significantly higher seed viability than in the Pt-S tumors, was also reflected in the change in seed composition (insert in **Fig. 5E**). These data suggest that it is not an individual miRNA but a combination of nontoxic miRNAs that confers Pt resistance in human ovarian cancer.

The average 6mer seed composition of total RISC-bound miRNAs in the tumors revealed differences between patients (Supplementary Fig. S7). The average seed composition of 8 of the tumors started with AAC (red boxes in Supplementary Fig. S7) and of 11 started with AGC (green boxes in Supplementary Fig. S7). This is likely due to a predominance of either miR-141/200a-3p (6mer seed: AACACU) and miR-21–5p (AGCUUA) in either group, respectively. These miRNAs are two of the most abundant miRNAs in the RISC of the analyzed ovarian cancer tumors. However, both subtypes were represented in Pt-S and Pt-R patients and, therefore, do not correlate with outcome.

When focusing on only the most highly expressed miRNAs in Pt-R patient tumors, we found six miRNAs to correlate with Pt resistance inpatients with ovarian cancer (Supplementary Table S4). Grouping patients with the 50% highest and lowest combined reads of these six
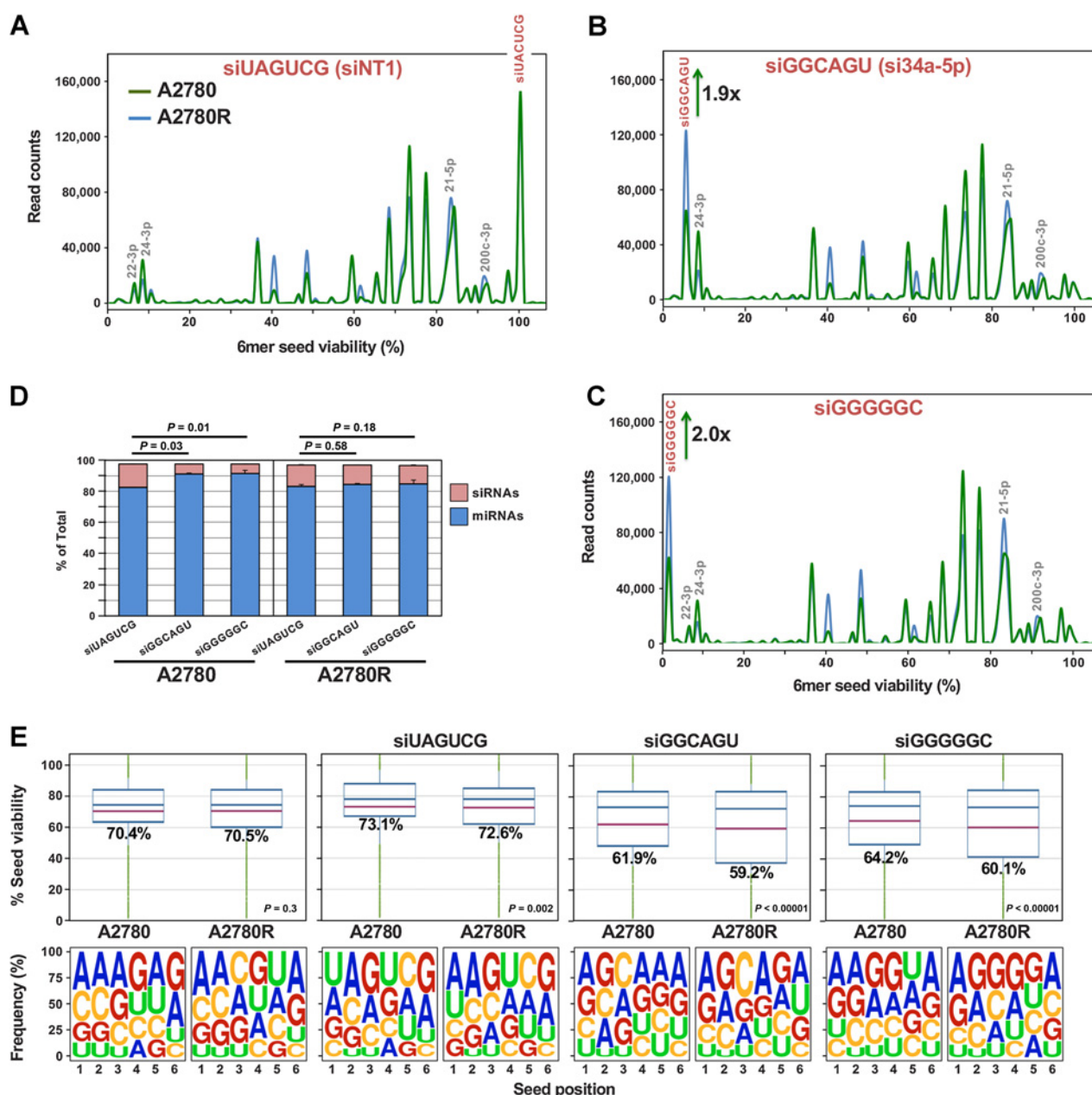
Figure 4.
Platinum-resistant A2780R cells have more toxic miRNAs in their RISC than sensitive A2780 cells. **A–C,** Seed tox graph of RISC-bound miRNAs and exogenous siRNAs in A2780/A2780R cells 24 hours after transfection with either the nontoxic siUAGUCG (siNT1), or the highly toxic siGGCAGU, or siGGGGGC. **D,** Percent miRNAs and exogenous siRNAs in the RISC of the siRNA-transfected cells. Student test *P* values are shown on the change in percent of transfected siRNAs. **E,** Average seed tox (top) and seed composition (bottom) of all RISC-bound sRNAs in A2780/A2780R cells PBS treated or treated with the three siRNAs. *P* values were calculated using a Wilcoxon rank test. The fraction of exogenous siRNAs and endogenous miRNAs was approximately 97% in all samples.

miRNAs separated Pt-S from Pt-R patients (**Fig. 5F**). These six highly abundant miRNAs also correlated individually with the Pt-sensitive days (**Fig. 5G**). Individual Kaplan–Meier analyses with these six miRNAs showed that the separation is largely driven by four miRNAs (miR-125a-5p, miR-125b-5p, miR-100–5p, and miR-199–5p). Using the combination of these miRNAs allowed the best distinction between Pt-S and Pt-R patients (Supplementary Fig. S8).

Analysis of primary tumors and recurrences in patients with very long overall survival

A comparison of matched primary tumors with recurrences is often not feasible in ovarian cancer, because patients are usually only operated on once. However, we recently described a subgroup of patients who, for unknown reasons, maintain Pt sensitivity and/or have oligometastatic recurrences (45, 46). Because some of these
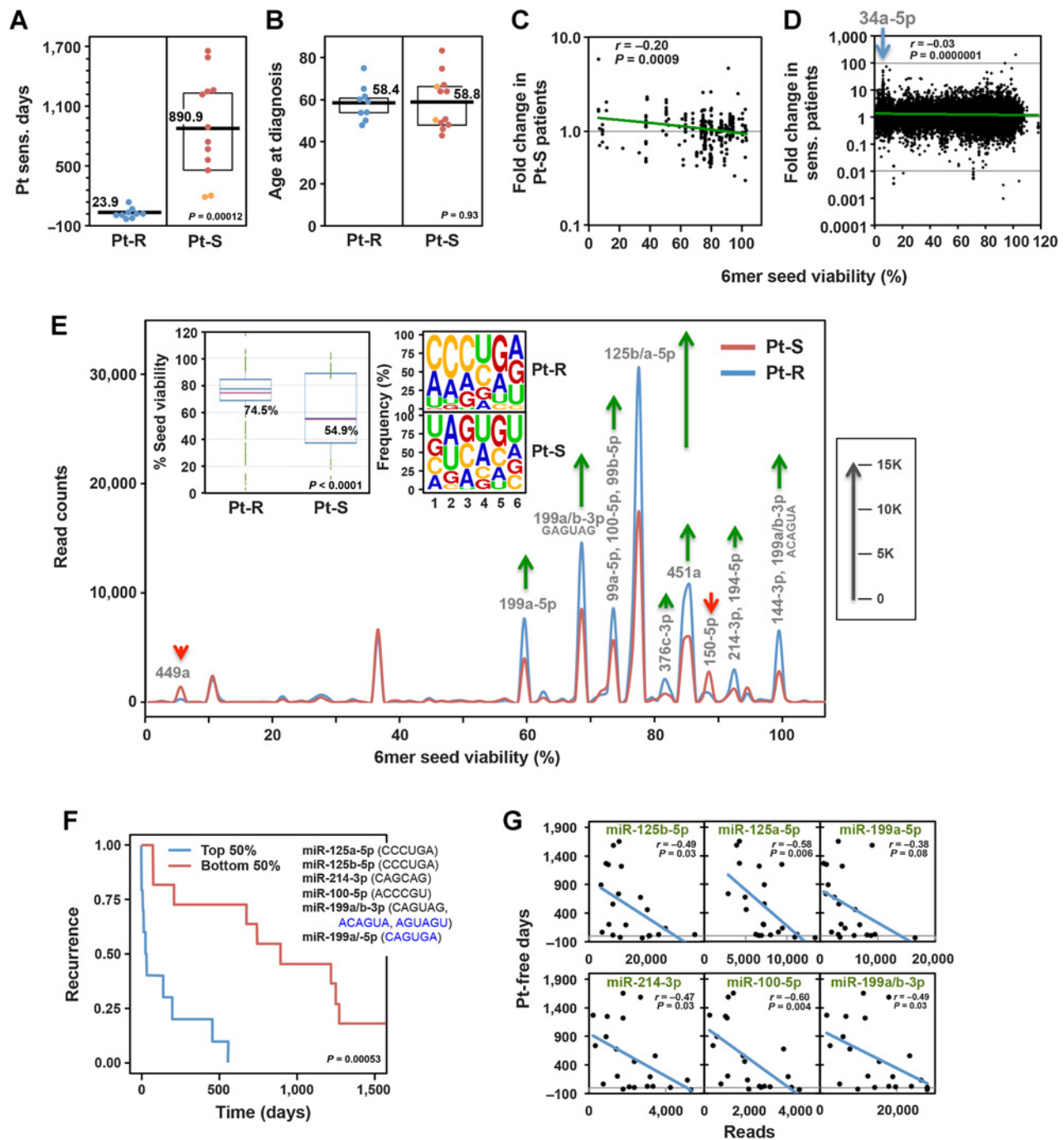
Figure 5.
Lower seed tox of RISC-bound sRNAs in ovarian cancer tumors is associated with increased resistance to chemotherapy. **A,** Pt-sensitive days (days between the end of the last cycle of Pt-based chemotherapy and first relapse) in two groups of patients with ovarian cancer: Pt-R and Pt-S. Orange dots indicate two patients with intermediate (180 to 365 days since last treatment) Pt sensitivity. **B,** Differences in age at diagnosis between the two groups in **Fig. 5A**. Kruskal–Wallis median test P values are shown. **C,** Pearson correlation between the fold change in Pt-S versus Pt-R patients and the 6mer seed tox (% viability in HeyA8 cells). Shown are miRNAs with a sum of >10,000 across all samples (representing 85.4% of all reads). miRNA content of this pull down was 97.4% to 98.1%. **D,** Pearson correlation between the fold change in Pt-S versus Pt-R patients and the 6mer seed tox (% viability in HeyA8 cells). Shown are all approximately 38,000 different reads across all samples. The position of a number of reads representing miR-34a-5p highly enriched in the Pt-S cells is indicated. Note, these reads while highly upregulated, did not reach statistical significance in the fold-change analyses. **E,** Seed tox graph of RISC-bound miRNAs differentially expressed ($P < 0.05$, >1.5x fold change) in Pt-S versus Pt-R patients. Green arrows, net increase, and red arrows, net decrease of >1,000 reads in peak in Pt-R tumors, respectively. Insets, left, average seed tox of all sRNAs enriched in either Pt-R or Pt-S patients. Right, matching seed compositions. **F,** Kaplan–Meier analysis of patients with the top and bottom highest RISC content of the average of the six miRNAs shown (including their 6mer seeds). Noncanonical seeds are in blue. **G,** Regression analysis of the six miRNAs in **D** plotted against the number of Pt-S days.
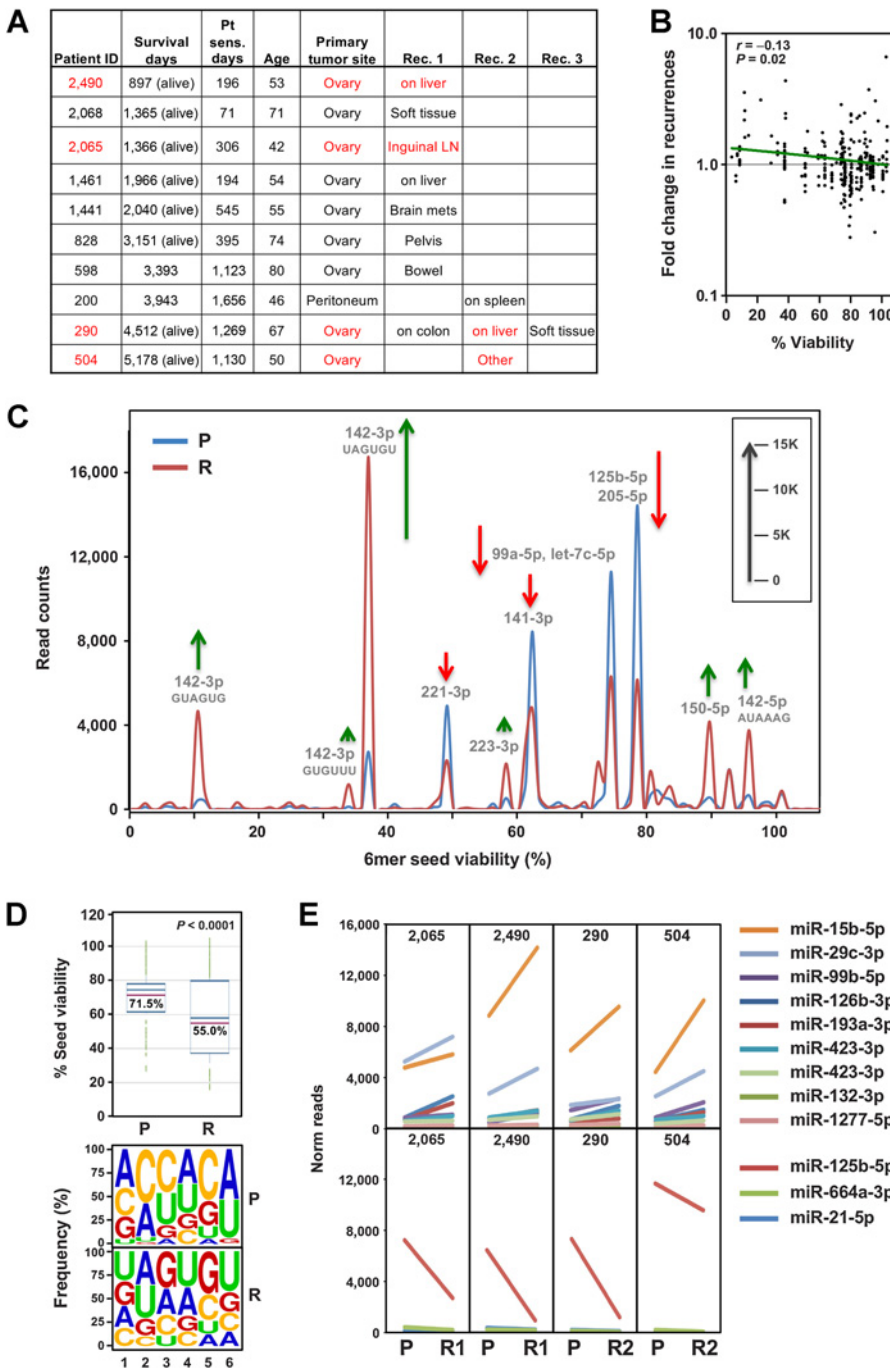
Figure 6.
The RISC in recurrent ovarian cancer tumors in a group of long-term survivors is enriched in miRNAs with toxic 6mer seeds compared with the primary cancer. **A,** List of 10 long-term survivor ovarian cancer patients with sites of recurrences given. Patient pairs of a subgroup of four highly related primary and recurrent tumor pairs are shown in red (see Supplementary Fig. S9F). Survival days are as of December 22, 2020. **B,** Pearson correlation between the fold change in recurrences versus primary tumors and the 6mer seed tox (% viability in HeyA8 cells). Shown are miRNAs with a sum of >10,000 across all samples (representing 81.4% of all reads). miRNA content of this pull down was 97.2% to 98.4%. **C,** Seed tox graph of RISC-bound miRNAs differentially expressed (paired analysis, $P < 0.05$, >1.5× fold change) in recurrences versus matched primary tumors in the subgroup of four patients. Note, miR-15b-5p was not detected in this analysis, which used the EdgeR software package to obtain paired P values and it had a P value of 0.057. Green arrows, net increase, and red arrows, net decrease of >1,000 reads in peak in recurrent tumors, respectively. **D,** Top, average seed tox of all sRNAs enriched in either primary tumor (P) or recurrences (R). Bottom, matching seed compositions. **E,** Changes in RISC-bound miRNA read numbers in recurrences versus primary tumors in the subgroup of patients. Shown are all miRNAs that are significantly up- (top) or downregulated (bottom; paired Student t test $P < 0.05$, >1.5× fold) in all four patients in the same direction.

patients undergo a secondary surgery, we were able to compare 6mer seed tox between the initial tumor and the recurrence (**Fig. 6A**; Supplementary Table S3). Two patients (#290 and #200) overlapped with the above analysis (Supplementary Fig. S9A–S9D); however, we analyzed a different tumor site, which allowed us to test both the similarities between these tumors and the reproducibility of the Ago pull down/smRNA-seq analysis. The independent analyses of the two tumors from the same patients were more similar when compared with the average of the other primary tumors in the second set (Supplementary Fig. S9B–S9D).

Overall seed tox was significantly higher in the recurrent tumors based on a comparison of the most abundant reads in the matched primary tumors (**Fig. 6B**). Integrating all reads of the primary tumors and the recurrences revealed that some miRNAs with toxic seeds were upregulated (e.g., miR-22–3p and the miR-15/16–5p family), while miRNAs with nontoxic seeds (miR-26a/b-5p, let-7–5p family, miR-143–5p, miR-125a/b-5p, miR-30–5p family) were downregulated in the recurrent tumors and this resulted in a moderate yet significant reduction in average seed toxicity of the RISC-bound sRNAs in the recurrences (Supplementary Fig. S9E and inset). While the recurrences

and primary tumors were from the same patients, we could not exclude the possibility that the difference in seed tox of RISC-bound miRNAs was due to differences in the tumor microenvironment or the distinct anatomic locations of the first and second surgery. However, an unsupervised hierarchical cluster analysis based on RISC-bound miRNAs identified the primary and recurrent tumors from four patients as highly related regardless of anatomic location, suggesting that the detected miRNAs were tumor-specific (Supplementary Fig. S9F). A seed tox graph was generated of the samples of these four tumor pairs (**Fig. 6C**). A few miRNAs with toxic seeds were upregulated in the recurrences, while several miRNAs (e.g., miR-125b-5p) with nontoxic seeds were downregulated. This resulted in a significant drop in average toxicity of all miRNAs enriched in recurrences (**Fig. 6D**). To identify the miRNAs driving these changes, we plotted all miRNAs that were significantly deregulated in the same direction in this subgroup of patients (**Fig. 6E**). In this analysis, in which we applied a paired Student t test, in three out of 4 patients, the most abundant upregulated miRNA was miR-15b-5p, which can kill cancer cells through 6mer seed tox (24), and the most abundant downregulated nontoxic miRNA was, again, miR-125b-5p. Analysis of all patient tumor pairs suggests that the differences seen between primary tumors and matched recurrences in this rare patient population are due to intrinsic changes in the tumor cells. Tumors of "multiple Pt responders" (47), do not acquire Pt resistance through upregulation of nontoxic/protective miRNAs. On the basis of our data, we predict that the recurrences in these patients will be as Pt sensitive as the initial tumors.

Discussion

We have recently advanced a novel concept to explain how miRNA families target gene networks that regulate cell fate (20, 21, 31, 48). This concept is not based on the activity of any individual miRNA or its

targets, but on the conclusion that it is the incidence of 6mer seed tox in all miRNAs present that determines whether genes critical for cell survival are being silenced. We are now proposing that the balance between miRNAs with highly toxic seeds and miRNAs that carry nontoxic seeds is predictive of treatment outcome in ovarian cancer. Testing this concept required assessing position 2–7 of RISC-bound miRNA guides. To obtain this information, we combined the method of Ago pull down/smRNA Seq with a specific bioinformatics pipeline to analyze 6mer seeds in short reads. Our method does not involve crosslinking of the miRNAs with their target mRNAs, since the primary goal of this study was not to identity miRNA targets, but to determine the seed content of the RISC in cancer cells and tumor tissue. Recent data suggest that many miRNAs detected in total RNA are part of a low-molecular-weight RISC that is not associated with either GW182 or mRNAs (44). By using a GW182 peptide to pull down Ago proteins, we may have preferentially isolated active RISC complexes, as only those active (high-molecular-weight) complexes are comprised of miRNA, Ago, mRNAs, and GW182 (44). This is supported by our recent observation that the GW182 peptide could not efficiently pull down Ago in Drosha KO cells devoid of most miRNAs (23) despite unchanged Ago expression levels (20). It also provides an explanation for the large variation we found between total and RISC-bound miRNAs for a number of miRNAs. Ago proteins are stabilized by bound miRNAs and the number of mRNAs with targeted seed matches that bind to these miRNAs (43). Our finding that the two toxic siRNAs, siGGCAGU and siGGGGGC, are present in higher numbers and loaded into the RISC more efficiently than the nontoxic siUAGUCG when transfected into the A2780R cells, could be because the two toxic siRNAs target survival/housekeeping genes in this cell line (23).

We developed a way to visualize all significantly expressed miRNAs in one simple graph. The 6mer seed tox graph relies only on the predicted toxicity of every miRNA based on our screen of all 6mer

Figure 7.
Scheme to illustrate the balance of toxic RISC-bound miRNAs that determine platinum sensitivity. In constitutively Pt-S ovarian cancer cells, treatment with Pt results in a shift in the ratio of miRNAs with toxic and nontoxic seeds tipping the balance toward cell death (death induced by survival gene elimination, DISE; **I**). In ovarian cancer cells with acquired Pt resistance, the shift toward toxic seed–containing miRNAs is insufficient to trigger DISE (**II**). However, the protection by miRNAs with nontoxic seeds can be overcome by introducing exogenous miRNA mimetics (e.g., siGG-CAGU = si34a-5p) that contain highly toxic seeds (**III**). Finally, inhibiting miRNAs with nontoxic seeds, as shown for overexpressed miR-21-5p (using a miR-21-5p inhibitor, miR-21i) in the A2780R cells, allows the Pt-R cells (both constitutively as well as acquired) to regain sensitivity to Pt (**IV**).
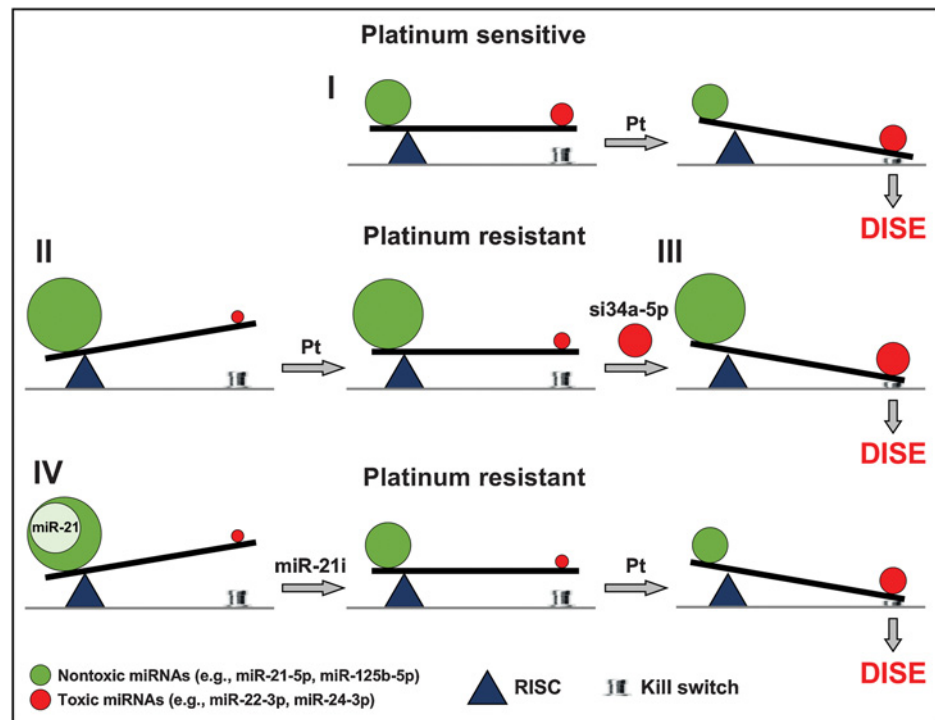
seeds. miRNAs that are part of different families with entirely different biological functions may have similar seed toxicities and will be found in the same peaks. Based on these analyses, we are proposing that it is the balance between toxic and nontoxic 6mers embedded in miRNAs that predicts whether cancer cells die or resist Pt-based chemotherapy (**Fig. 7**). We provide the first evidence that efficient Pt induced cell death is in part dependent on a functional RNAi system and that cells devoid of miRNAs (most of which contain nontoxic seeds) are highly sensitive to Pt induced cell death. The immediate reaction of ovarian cancer cells to Pt is downregulation of miRNAs with nontoxic seeds and upregulation of miRNAs containing highly toxic 6mer seeds such as miR-22–3p and miR-24–3p (**Fig. 7I**). Both of these miRNAs are upregulated in human embryonic stem cells lines upon differentiation (49) and both have been shown to induce cell death when transfected into HCT116 cells (50). In contrast, ovarian cancer cells that have acquired resistance after long-term Pt exposure show the opposite pattern: These Pt-R cells contain fewer toxic miRNAs and more nontoxic RISC-associated miRNAs (**Fig. 7, II**). However, this resistance can be overcome by introducing artificial miRNAs with highly toxic seeds (e.g., siGGGGGC or siGGCAGU; **Fig. 7, III**). Finally, when the nontoxic miRNAs are predominately one species (e.g., miR-21–5p in the A2780R cells) inhibiting this miRNA can re-sensitize cells to treatment (**Fig. 7, IV**). Consistent with the *in vitro* data, tumors from patients with Pt resistance had more miRNAs with nontoxic seeds, while Pt-sensitive patients had more miRNAs with toxic seeds. Confirming the proposed concept, recurrent tumors from patients that remain Pt sensitive had higher concentrations of toxic miRNAs in their RISC compared with the original primary tumor. In both analyses of patient tumors, the nontoxic miRNA most relevant to primary ovarian cancer tumors was the abundant miRNA miR-125b-5p.

While our study is based on a relatively small number of patients, this is the first analysis of primary human tumors based exclusively on RISC-bound miRNAs. Traditionally, analysis of miRNAs in human cancers is done using total RNA. It is based on the assumption that quantification of total miRNA amounts in cells or tissue allows the assessment of the functional relevance of expressed miRNAs. Yet, a recent study has shown that the level of Ago-bound miRNAs is a better indicator of miRNA activity than the total level of miRNA expression. The differential binding of miRNAs to the RISC was found to be cell type specific (43), and to be independent of GC content of miRNAs. However, it was strongly dependent on the abundance of complementary mRNA targets. Our data now suggest this is true of ovarian tumors. We identify a number of miRNAs that are preferentially associated with Ago proteins, some of which we then found to be associated with the response of ovarian cancer cells to Pt-based chemotherapy.

While there are many mechanisms that determine Pt resistance of OC such as DNA repair or cancer stem cells (16, 17), miRNAs have been shown to regulate these processes and to play important roles as evidenced by the large number of reports describing miRNAs as regulators and clinical predictors of treatment outcome in this disease (see our analysis in Supplementary Tables S1 and S2). However, our data suggest that focusing on single miRNAs or even miRNA families will not result in a reliable marker for Pt-resistant ovarian cancer. We hypothesize that ovarian cancer cells can acquire Pt resistance by upregulating any miRNA that carries a nontoxic 6mer seed. This hypothesis is consistent with the countless reports that provide evidence for the involvement of single miRNAs in Pt resistance in ovarian cancer cell lines (51–59) (Supplementary Tables S1 and S2). Pt resistance in different ovarian cancer cell line models and in patients with ovarian cancer may be driven by a variety of nontoxic miRNAs. This is supported by our smRNAseq data derived from different models (Supplementary Table S5). We conclude that Pt resistance in each of the models and in human patients may be driven by different nontoxic miRNAs reported to render ovarian cancer cells Pt tolerant. Our cisplatin resistant A2780R utilize miR-21–5p and PEO4 cells are more tolerant to carboplatin due, in part, to upregulation of miR-130a-3p. Finally, in tumors from Pt-R patients, we found evidence for an upregulation of RISC-bound miR-214–3p and, most prominently, miR-125b-5p in the most Pt resistant patients. While any of these miRNAs could serve as targets for therapy and as biomarkers, it is entirely possible that different miRNAs will be identified that confer therapy resistance in other cell lines and patient analyses. What they may all share is the presence of a nontoxic seed. Artificial toxic 6mer seed containing miRNAs or siRNAs could therefore be used to eliminate ovarian cancer and other cancers. Indeed, our data suggest that Pt-resistant tumors may be at least as sensitive to these toxic siRNAs as chemotherapy-sensitive tumors.

Authors' Contributions

M. Patel: Formal analysis, investigation, writing–review and editing. **Y. Wang:** Investigation. **E.T. Bartom:** Data curation, formal analysis. **R. Dhir:** Resources. **K.P. Nephew:** Resources. **D. Matei:** Resources, supervision. **A.E. Murmann:** Investigation. **E. Lengyel:** Resources, supervision, writing–review and editing. **M.E. Peter:** Conceptualization, data curation, formal analysis, supervision, funding acquisition, writing–original draft, project administration, writing–review and editing.

References

1. Alles J, Fehlmann T, Fischer U, Backes C, Galata V, Minet M, et al. An estimate of the total number of true human miRNAs. Nucleic Acids Res 2019; 47:3353–64.

2. Yan M, Yang X, Shen R, Wu C, Wang H, Ye Q, et al. miR-146b promotes cell proliferation and increases chemosensitivity, but attenuates cell migration and invasion via FBXL10 in ovarian cancer. Cell Death Dis 2018;9:1123.

3. Svoronos AA, Engelman DM, Slack FJ. OncomiR or tumor suppressor? the duplicity of MicroRNAs in cancer. Cancer Res 2016;76:3666–70.

4. Chan JK, Blansit K, Kiet T, Sherman A, Wong G, Earle C, et al. The inhibition of miR-21 promotes apoptosis and chemosensitivity in ovarian cancer. Gynecol Oncol 2014;132:739–44.

5. Lewis BP, Shih IH, Jones-Rhoades MW, Bartel DP, Burge CB. Prediction of mammalian microRNA targets. Cell 2003;115:787–98.

6. Lai EC. Micro RNAs are complementary to 3′ UTR sequence motifs that mediate negative post-transcriptional regulation. Nat Genet 2002;30:363–4.

7. Selbach M, Schwanhausser B, Thierfelder N, Fang Z, Khanin R, Rajewsky N. Widespread changes in protein synthesis induced by microRNAs. Nature 2008; 455:58–63.

8. Baek D, Villen J, Shin C, Camargo FD, Gygi SP, Bartel DP. The impact of microRNAs on protein output. Nature 2008;455:64–71.

9. Eulalio A, Huntzinger E, Izaurralde E. GW182 interaction with argonaute is essential for miRNA-mediated translational repression and mRNA decay. Nat Struct Mol Biol 2008;15:346–53.

10. Wang Y, Sheng G, Juranek S, Tuschl T, Patel DJ. Structure of the guide-strand-containing argonaute silencing complex. Nature 2008;456:209–13.

11. Leuschner PJ, Ameres SL, Kueng S, Martinez J. Cleavage of the siRNA passenger strand during RISC assembly in human cells. EMBO Rep 2006;7:314–20.

12. Bast RC Jr, Matulonis UA, Sood AK, Ahmed AA, Amobi AE, Balkwill FR, et al. Critical questions in ovarian cancer research and treatment: report of an american association for cancer research special conference. Cancer 2019;125: 1963–72.

13. Integrated genomic analyses of ovarian carcinoma. Nature 2011;474:609–15.

14. Kurnit KC, Fleming GF, Lengyel E. Updates and new options in advanced epithelial ovarian cancer treatment. Obstet Gynecol 2020.

15. Agarwal R, Kaye SB. Ovarian cancer: strategies for overcoming resistance to chemotherapy. Nat Rev Cancer 2003;3:502–16.

16. Norouzi-Barough L, Sarookhani MR, Sharifi M, Moghbelinejad S, Jangjoo S, Salehi R. Molecular mechanisms of drug resistance in ovarian cancer. J Cell Physiol 2018;233:4546–62.

17. Christie EL, Bowtell DDL. Acquired chemotherapy resistance in ovarian cancer. Ann Oncol 2017;28:viii13–viii5.

18. Hadji A, Ceppi P, Murmann AE, Brockway S, Pattanayak A, Bhinder B, et al. Death induced by CD95 or CD95 ligand elimination. Cell Rep 2014;10:208–22.

19. Murmann AE, McMahon KM, Halluck-Kangas A, Ravindran N, Patel M, Law C, et al. Induction of DISE in ovarian cancer cells in vivo. Oncotarget 2017;8: 84643–58.

20. Putzbach W, Gao QQ, Patel M, van Dongen S, Haluck-Kangas A, Sarshad AA, et al. Many si/shRNAs can kill cancer cells by targeting multiple survival genes through an off-target mechanism. eLife 2017;6:e29702.

21. Patel M, Bartom ET, Murmann AE, Peter ME. Identification of the toxic 6mer seed consensus in human cancer cells. BioRxive 2020:12.22.424040.

22. Corbin JM, Geordescu C, wren JD, Xu C, Asch AS, Ruiz-Echevarria MJ. Seed-mediated RNA interference of androgen signaling and survival networks induces cell death in prostate cancer cells. Molecular Therapy Nucleic Acids 2021;24: 337–51.

23. Gao QQ, Putzbach W, Murmann AE, Chen S, Ambrosini G, Peter JM, et al. 6mer seed toxicity in tumor suppressive miRNAs. Nature Comm 2018;9:4504.

24. Murmann AE, Bartom ET, Schipma MJ, Vilker J, Chen S, Peter ME. 6mer seed toxicity in viral microRNAs. iScience 2019;23:100737.

25. Gu D, Ahn SY, Eom S, Lee HS, Ham J, Lee DH, et al. AGO-accessible anticancer siRNAs designed with synergistic miRNA-like activity. Molecular Therapy Nucleic Acids 2021;23:1172–90.

26. Ceppi P, Hadji A, Kohlhapp F, Pattanayak A, Hau A, Xia L, et al. CD95 and CD95L promote and protect cancer stem cells. Nature Commun 2014;5: 5238.

27. Wang Y, Zong X, Mitra S, Mitra AK, Matei D, Nephew KP. IL-6 mediates platinum-induced enrichment of ovarian cancer stem cells. JCI insight 2018;3: e122360.

28. Bogerd HP, Whisnant AW, Kennedy EM, Flores O, Cullen BR. Derivation and characterization of dicer- and microRNA-deficient human cells. RNA 2014;20: 923–37.

29. Eckenfelder A, Segeral E, Pinzon N, Ulveling D, Amadori C, Charpentier M, et al. Argonaute proteins regulate HIV-1 multiply spliced RNA and viral production in a dicer independent manner. Nucleic Acids Res 2017;45:4158–73.

30. van Eijl R, van den Brand T, Nguyen LN, Mulder KW. Reactivity of human AGO2 monoclonal antibody 11A9 with the SWI/SNF complex: a case study for rigorously defining antibody selectivity. Sci Rep 2017;7:7278.

31. Putzbach W, Haluck-Kangas A, Gao QQ, Sarshad AA, Bartom ET, Stults A, et al. CD95/Fas ligand mRNA is toxic to cells. eLife 2018;7:e38621.

32. Hauptmann J, Schraivogel D, Bruckmann A, Manickavel S, Jakob L, Eichner N, et al. Biochemical isolation of argonaute protein complexes by Ago-APP. Proc Natl Acad Sci U S A 2015;112:11841–5.

33. Hafner M, Renwick N, Farazi TA, Mihailovic A, Pena JT, Tuschl T. Barcoded cDNA library preparation for small RNA profiling by next-generation sequencing. Methods 2012;58:164–70.

34. Blayney JK, Davison T, McCabe N, Walker S, Keating K, Delaney T, et al. Prior knowledge transfer across transcriptional data sets and technologies using compositional statistics yields new mislabelled ovarian cell line. Nucleic Acids Res 2016;44:e137.

35. Pirker R, FitzGerald DJ, Hamilton TC, Ozols RF, Willingham MC, Pastan I. Anti-transferrin receptor antibody linked to pseudomonas exotoxin as a model immunotoxin in human ovarian carcinoma cell lines. Cancer Res 1985;45: 751–7.

36. Anglesio MS, Wiegand KC, Melnyk N, Chow C, Salamanca C, Prentice LM, et al. Type-specific cell line models for type-specific ovarian cancer research. PLoS One 2013;8:e72162.

37. Mitra AK, Davis DA, Tomar S, Roy L, Gurler H, Xie J, et al. In vivo tumor growth of high-grade serous ovarian cancer cell lines. Gynecol Oncol 2015;138:372–7.

38. Wang Y, Zhao G, Condello S, Huang H, Cardenas H, Tanner EJ, et al. Frizzled-7 identifies platinum tolerant ovarian cancer cells susceptible to ferroptosis. Cancer Res 2020.

39. Li M, Balch C, Montgomery JS, Jeong M, Chung JH, Yan P, et al. Integrated analysis of DNA methylation and gene expression reveals specific signaling pathways associated with platinum resistance in ovarian cancer. BMC Med Genomics 2009;2:34.

40. Wolf CR, Hayward IP, Lawrie SS, Buckton K, McIntyre MA, Adams DJ, et al. Cellular heterogeneity and drug resistance in two ovarian adenocarcinoma cell lines derived from a single patient. Int J Cancer 1987;39:695–702.

41. Sakai W, Swisher EM, Jacquemont C, Chandramohan KV, Couch FJ, Langdon SP, et al. Functional restoration of BRCA2 protein by secondary BRCA2 mutations in BRCA2-mutated ovarian carcinoma. Cancer Res 2009; 69:6381–6.

42. Janas MM, Wang B, Harris AS, Aguiar M, Shaffer JM, Subrahmanyam YV, et al. Alternative RISC assembly: binding and repression of microRNA-mRNA duplexes by human ago proteins. RNA 2012;18:2041–55.

43. Flores O, Kennedy EM, Skalsky RL, Cullen BR. Differential RISC association of endogenous human microRNAs predicts their inhibitory potential. Nucleic Acids Res 2014;42:4629–39.

44. La Rocca G, Olejniczak SH, Gonzalez AJ, Briskin D, Vidigal JA, Spraggon L, et al. In vivo, argonaute-bound microRNAs exist predominantly in a reservoir of low molecular weight complexes not associated with mRNA. Proc Natl Acad Sci U S A 2015;112:767–72.

45. Javellana M, Hoppenot C, Lengyel E. The road to long-term survival: surgical approach and longitudinal treatments of long-term survivors of advanced-stage serous ovarian cancer. Gynecol Oncol 2019;152:228–34.

46. Hoppenot C, Eckert MA, Tienda SM, Lengyel E. Who are the long-term survivors of high grade serous ovarian cancer? Gynecol Oncol 2018;148:204–12.

47. Patch AM, Christie EL, Etemadmoghadam D, Garsed DW, George J, Fereday S, et al. Whole-genome characterization of chemoresistant ovarian cancer. Nature 2015;521:489–94.

48. Putzbach W, Gao QQ, Patel M, Haluck-Kangas A, Murmann AE, Peter ME. DISE - a seed dependent RNAi off-target effect that kills cancer cells. Trends Cancer 2018;4:10–9.

49. Stadler B, Ivanovska I, Mehta K, Song S, Nelson A, Tan Y, et al. Characterization of microRNAs involved in embryonic stem cell states. Stem Cells Dev 2010;19: 935–50.

50. Sastre D, Baiochi J, de Souza Lima IM, Canto de Souza F, Corveloni AC, Thome CH, et al. Focused screening reveals functional effects of microRNAs differentially expressed in colorectal cancer. BMC Cancer 2019;19:1239.

51. Echevarría-Vargas IM, Valiyeva F, Vivas-Mejía PE. Upregulation of miR-21 in cisplatin resistant ovarian cancer via JNK-1/c-Jun pathway. PLoS One 2014;9: e97094.

52. Vandghanooni S, Eskandani M, Barar J, Omidi Y. AS1411 aptamer-decorated cisplatin-loaded poly(lactic-co-glycolic acid) nanoparticles for targeted therapy of miR-21-inhibited ovarian cancer cells. Nanomedicine 2018;13:2729–58.

53. Kong F, Sun C, Wang Z, Han L, Weng D, Lu Y, et al. miR-125b confers resistance of ovarian cancer cells to cisplatin by targeting pro-apoptotic Bcl-2 antagonist killer 1. J Huazhong Univ Sci Technolog Med Sci 2011;31:543.

54. Li N, Yang L, Wang H, Yi T, Jia X, Chen C, et al. MiR-130a and MiR-374a function as novel regulators of cisplatin resistance in human ovarian cancer A2780 cells. PLoS One 2015;10:e0128886.

55. Xu M, Xiao J, Chen M, Yuan L, Li J, Shen H, et al. miR-149–5p promotes chemotherapeutic resistance in ovarian cancer via the inactivation of the hippo signaling pathway. Int J Oncol 2018;52:815–27.

56. Zhang J, Liu J, Xu X, Li L. Curcumin suppresses cisplatin resistance development partly via modulating extracellular vesicle-mediated transfer of MEG3 and miR-214 in ovarian cancer. Cancer Chemother Pharmacol 2017;79:479–87.

57. Jin P, Liu Y, Wang R. STAT3 regulated miR-216a promotes ovarian cancer proliferation and cisplatin resistance. Biosci Rep 2018;38:BSR20180547.

58. Wei Z, Liu Y, Wang Y, Zhang Y, Luo Q, Man X, et al. Downregulation of Foxo3 and TRIM31 by miR-551b in side population promotes cell proliferation, invasion, and drug resistance of ovarian cancer. Med Oncol 2016; 33:126.

59. Wu J, Zhang L, Wu S, Yi X, Liu Z. miR-194–5p inhibits SLC40A1 expression to induce cisplatin resistance in ovarian cancer. Pathol Res Pract 2020;216: 152979.